

Measured and Simulated Thermoelectric Properties of FeAs_{2-x}Se_x ($x = 0.30 - 1.0$): from Marcasite to Arsenopyrite Structure

Christopher J. Perez,¹ Kasey P. Devlin,¹ Callista M. Skaggs,² Xiaoyan Tan,^{2,3*} Corey E. Frank,³ Jackson R. Badger,¹ Chang-Jong Kang,⁴ Thomas J. Emge,³ Susan M. Kauzlarich,¹ Valentin Taufour,⁵ Gabriel Kotliar,⁴ Saul H. Lapidus,⁶ and Martha Greenblatt^{3*}

¹ Department of Chemistry, University of California, Davis, One Shields Ave., Davis, CA 95616, United States

² Department of Chemistry and Biochemistry, George Mason University, Fairfax, Virginia 22030, United States

³ Department of Chemistry and Chemical Biology, Rutgers, The State University of New Jersey, Piscataway, New Jersey 08854, United States.

⁴ Department of Physics and Astronomy, Rutgers, The State University of New Jersey, Piscataway, New Jersey 08854, United States.

⁵ Department of Physics, University of California, One Shields Avenue, Davis, California 95616, United States.

⁶ Advanced Photon Source, Argonne National Laboratory, Argonne, Illinois, 60439, United States

*Corresponding authors' s E-mail: xtan6@gmu.edu, greenbla@chem.rutgers.edu

Electronic Supplementary Information

List of Tables and Figures

Figure S1: Laboratory (Cu K α , $\lambda = 1.5406 \text{ \AA}$) PXRD patterns before and after SPS.

Figure S2: Laboratory (Cu K α , $\lambda = 1.5406 \text{ \AA}$) PXRD patterns of FeAs_{2-x}Se_x ($x = 0.30, 0.50, 0.60, 0.65, 0.75, 0.85, 1.0$).

Table S1. Fractional Positional Coordinates and Anisotropic Thermal Parameters for FeAs_{1.50}Se_{0.50}

Table S2: Rietveld refinement results from Synchrotron PXRD of FeAsSe

Figure S3: Topological and X-ray elemental maps for polycrystalline FeAsSe. Composition calculated from EMPA analysis and the polycrystalline sample provides the composition Fe_{1.023(6)}As_{0.97(3)}Se_{1.00(4)}.

Figure S4: BSE images of FeAs_{2-x}Se_x ($x = 0.30, 0.75, 0.85$) with Fe, As, and Se X-ray elemental maps.

Figure S5: Experimental data thermoelectric data for sintered pellets of FeAs_{2-x}Se_x ($x = 0.30, 0.75, 0.85$)

Figure S6: Carrier concentration and carrier mobility of FeAsSe sintered pellet.

Figure S7: Room temperature carrier concentration and mobility of FeAs_{2-x}Se_x.

Figure S8: The calculated electronic thermal conductivity of FeAsSe. Two different computational schemes, GGA(PBE) and mBJ, are provided for comparison.

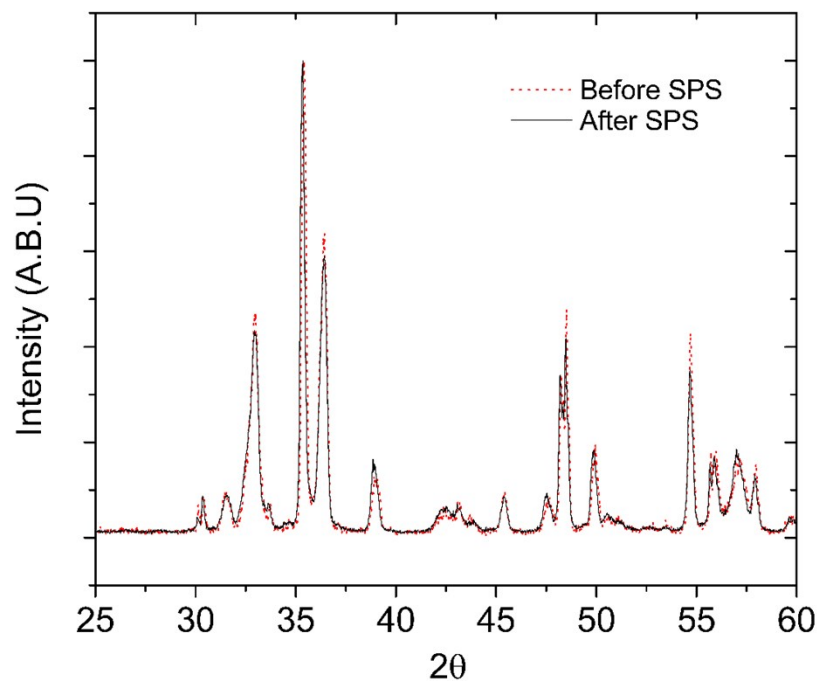


Figure S1: Laboratory (Cu $K\alpha$, $\lambda = 1.5406 \text{ \AA}$) PXRD patterns before and after SPS.

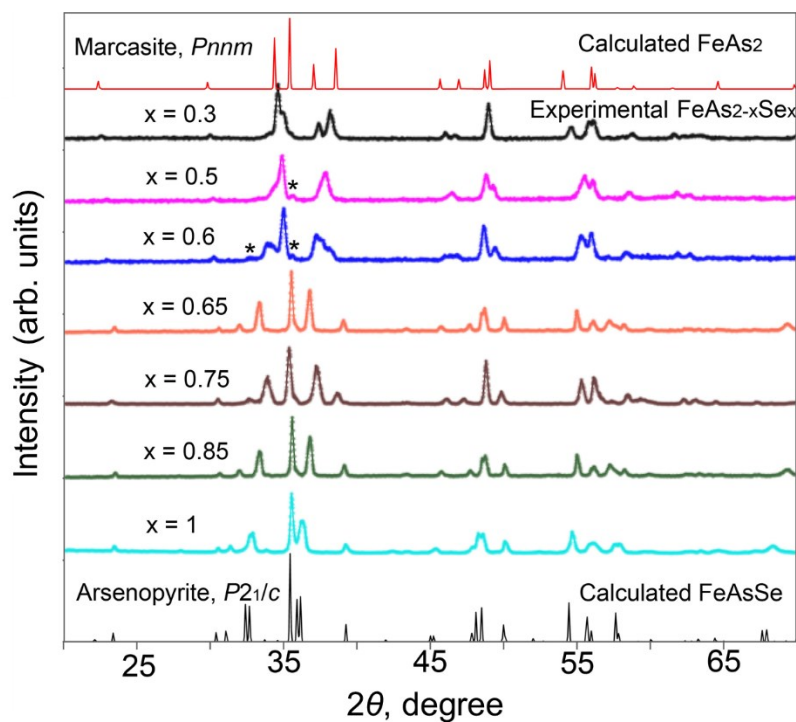


Figure S2: Laboratory PXRD (Cu $K\alpha$, $\lambda = 1.5406 \text{ \AA}$) patterns of $\text{FeAs}_{2-x}\text{Se}_x$ ($x = 0.30, 0.50, 0.60, 0.65, 0.75, 0.85, 1.0$). * represents the peaks of small amount of Arsenopyrite phase.

Table S1. Fractional Positional Coordinates and Anisotropic Thermal Parameters for FeAs_{1.50}Se_{0.50}

Label	Wyckoff Site	X	Y	Z	Occupancy	U ₁₁ (Å ²)	U ₂₂ (Å ²)	U ₃₃ (Å ²)	U ₂₃ (Å ²)	U ₁₃ (Å ²)	U ₁₂ (Å ²)
Fe1	2a	1/2	1/2	1/2	1.00	0.0039(5)	0.0025(5)	0.0091(5)	0	0	-0.0006(3)
As2	4g	0.31907(9)	0.13693(9)	1/2	0.75	0.0048(3)	0.0031(3)	0.0063(3)	0	0	-0.00047(14)
Se2	4g	0.31907(9)	0.13693(9)	1/2	0.25	0.0048(3)	0.0031(3)	0.0063(3)	0	0	-0.00047(14)

Table S2: Rietveld Refinement Results from Synchrotron PXRD of FeAsSe

	Comment
Nominal formula	FeAsSe
Wavelength (Å)	0.414532
temperature (K)	293 K
Space group	$P2_1/c$
Lattice Parameters <i>a, b, c, V</i>	$a = 5.95922(6)$ (Å), $b = 5.87517(6)$ (Å), $c = 5.99802(7)$ (Å), $V = 192.499$ Å ³ , $\beta = 113.5566(5)^\circ$
(R _F , GOF)	5.2, 2.1
Site	x, y, z
<i>Fe</i>	0.2720(5), -0.0013(5), 0.2813(4)
<i>As</i>	0.1509(3), 0.6312(3), 0.3666(3)
<i>Se</i>	0.3471(3), 0.3623(3), 0.1713(2)
<i>Fe (Occupancy)</i>	1
<i>As (Occupancy)</i>	1
<i>Se (Occupancy)</i>	0.970(5)

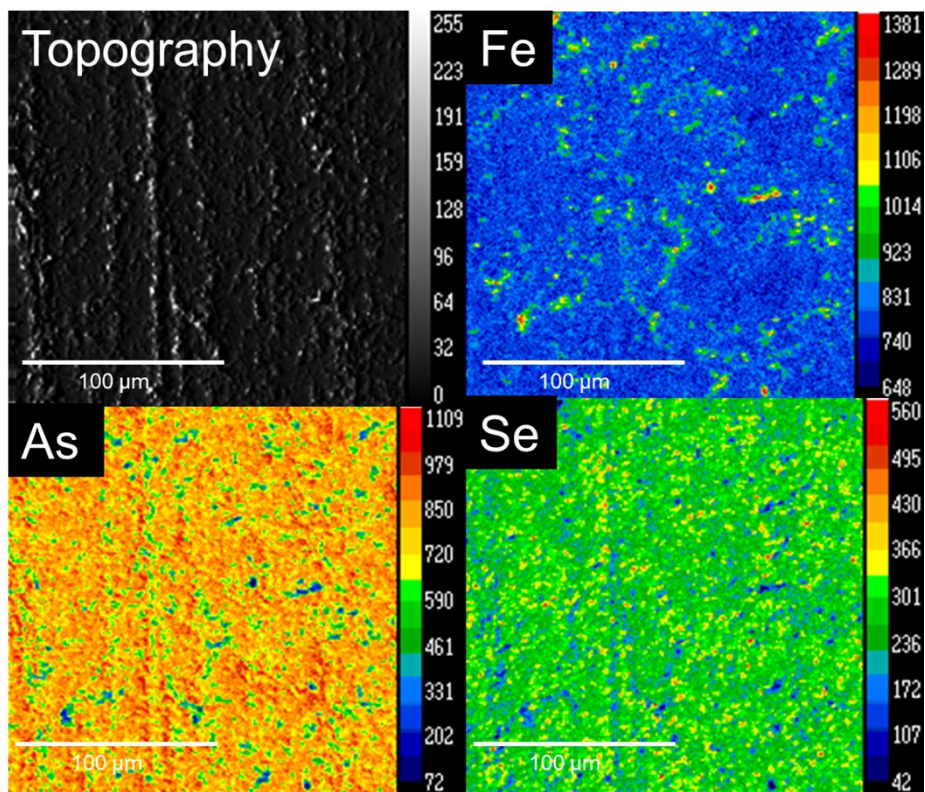


Figure S3: Topological and X-ray elemental maps for polycrystalline FeAsSe.

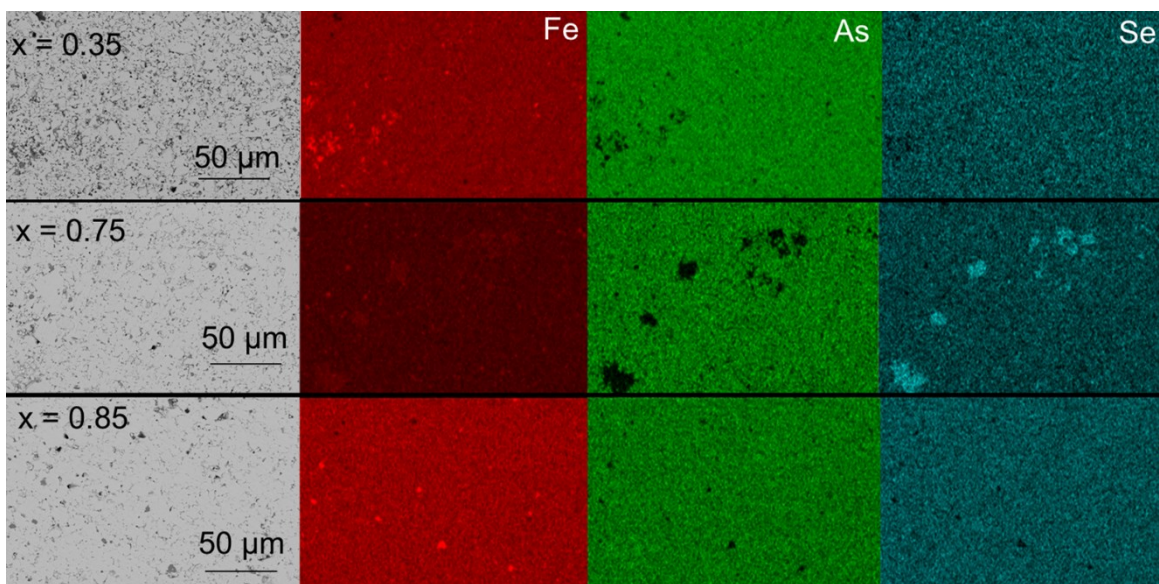


Figure S4: BSE images of $\text{FeAs}_{2-x}\text{Se}_x$ ($x = 0.30, 0.75, 0.85$) with Fe, As, and Se X-ray elemental maps.

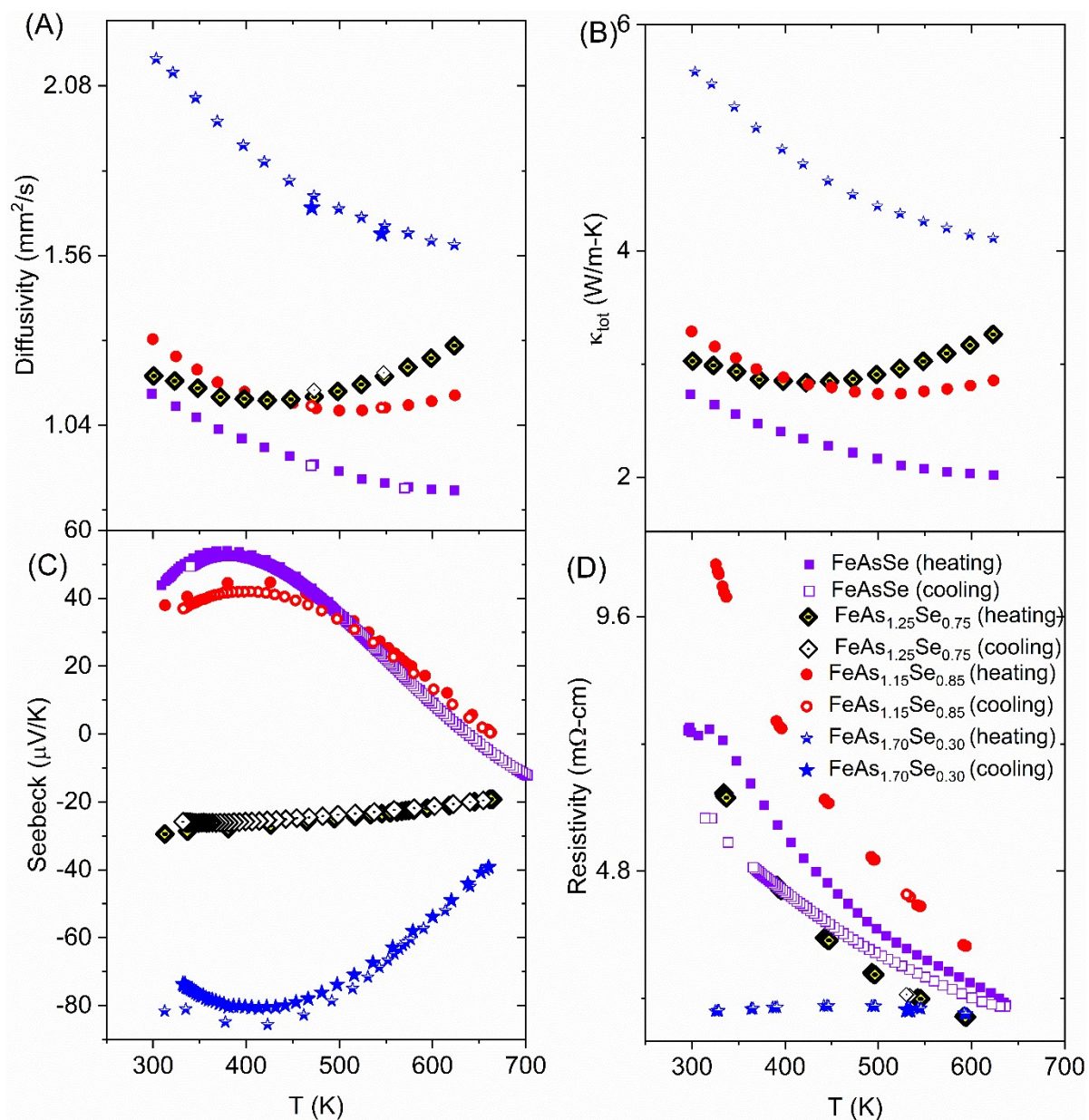


Figure S5: Thermally cycled experimental data showing (A) thermal diffusivity, (B) Thermal conductivity (C), Seebeck, and (D) resistivity for sintered pellets of $\text{FeAs}_{2-x}\text{Se}_x$ ($x = 0.30, 0.75, 0.85$).

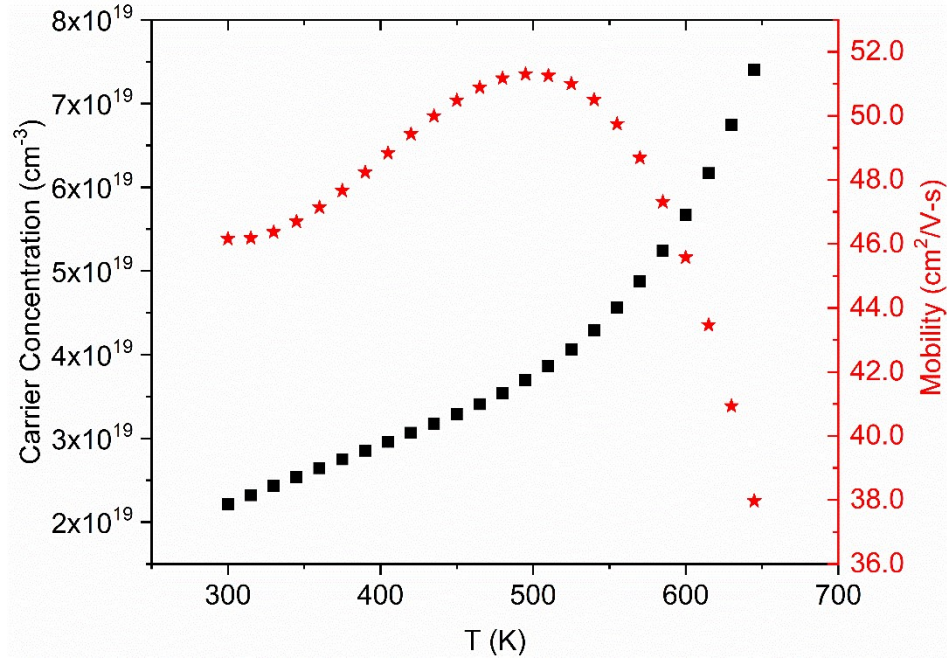


Figure S6: Carrier concentration and carrier mobility of FeAsSe measured on a sintered pellet.

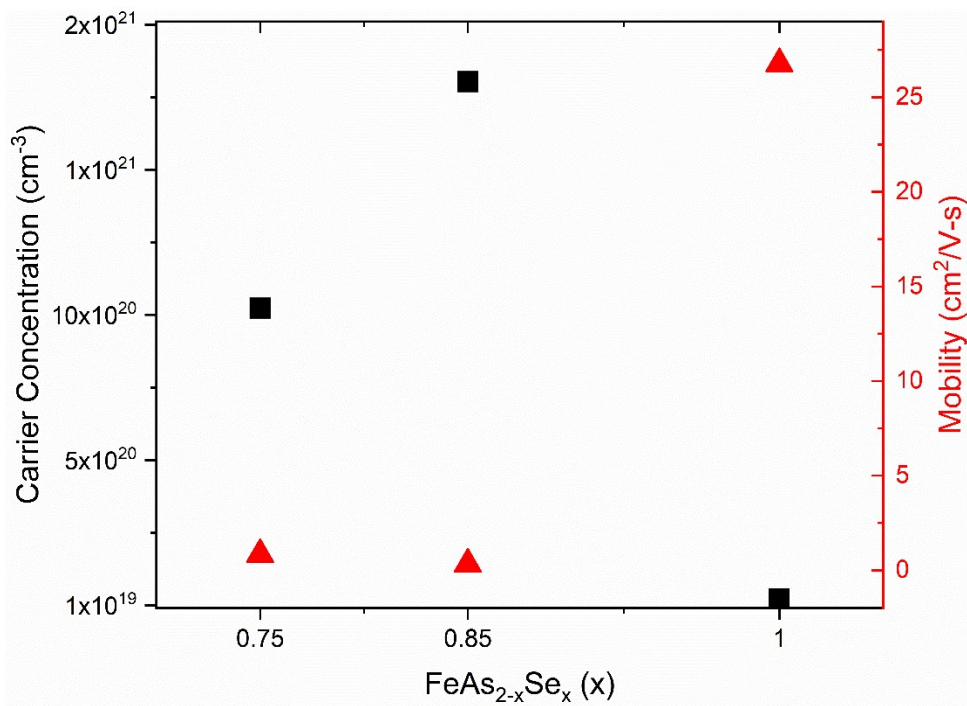


Figure S7: Room temperature carrier concentration and mobility of FeAs_{2-x}Se_x (x = 0.75, 0.85).

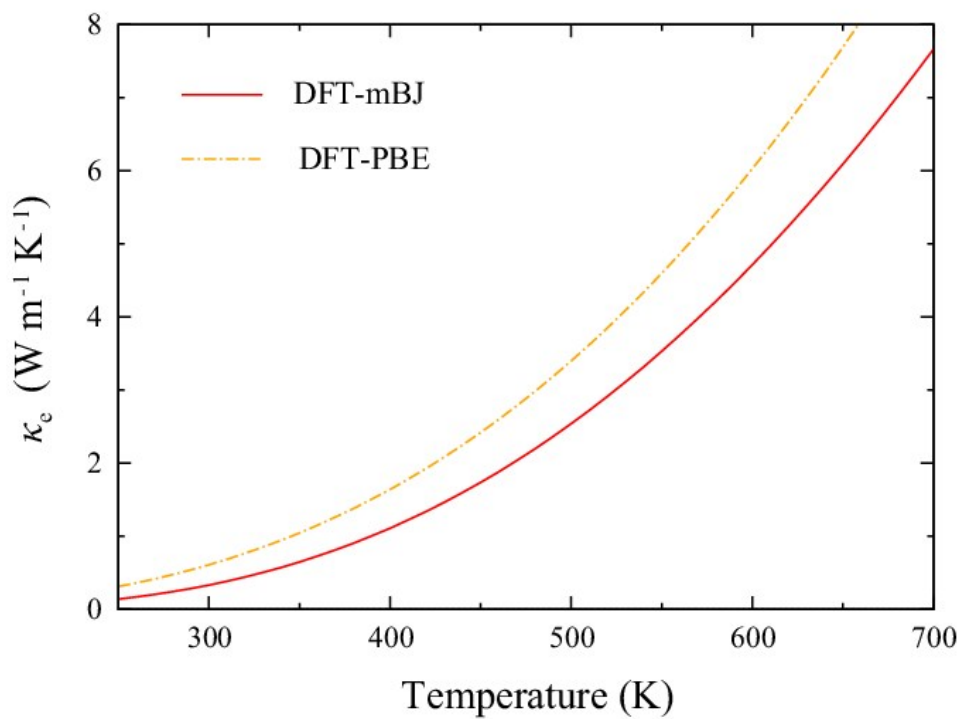


Figure S8: The calculated electronic thermal conductivity of FeAsSe. Two different computational schemes, GGA(PBE) and mBJ, are provided for comparison.